https://doi.org/10.5194/egusphere-2026-445
Preprint. Discussion started: 26 March 2026

Machine Learning vs. Conventional Methods for X-Band Radar Rainfall Estimation in Cyprus

Eleni Loulli[1,2], Silas Michaelides[1], and Diofantos G. Hadjimitsis[1,2]

[1]ERATOSTHENES Centre of Excellence, Limassol, Cyprus
[2]Department of Civil Engineering and Geomatics, Cyprus University of Technology, Limassol, Cyprus

Correspondence: Eleni Loulli (eleni.loulli@eratosthenes.org.cy)

Abstract. Polarimetric X-band radars offer high-resolution precipitation observations that are often challenged by attenuation, calibration errors, and absence of routine correction procedures, which limit reliable quantitative precipitation estimation (QPE). This study proposes a two-stage machine learning framework for estimating near-surface rainfall from the Cyprus national X-band radar network. In the first stage (Stage 1), feedforward neural networks correct raw ground radar reflectivity using volume-matched Ku-band measurements from the Global Precipitation Measurement (GPM) Mission dual-frequency precipitation radar (DPR). In the second stage (Stage 2), the corrected reflectivity is used as input to regression models, including support vector regression (SVR) and neural networks, to estimate rainfall rates using tipping-bucket rain gauge data. Results show that the Stage 1 networks substantially improve ground radar reflectivity, while Stage 2 SVR models outperform traditional Z–R relationships in predicting rainfall, despite residual underestimation and moderate accuracy. The study highlights the potential of machine learning methods for X-band radar QPE in environments with limited calibration and emphasizes the benefit of combining multiple radar datasets to improve spatial consistency. These findings provide practical insights for enhancing rainfall estimation in Cyprus and other regions with similar radar network constraints.

List of Abbreviations

Abbreviation	Meaning
ANN	Artificial Neural Network
AWS	Automatic Weather Station
BN	Bayesian Network
CNN	Convolutional Neural Network
DSD	Drop Size Distribution
DPR	Dual-frequency Precipitation Radar
FS	Full Swath
GPM	Global Precipitation Measurement
HB	Hitchfeld-Bordan technique
HS	High Sensitivity Scan

https://doi.org/10.5194/egusphere-2026-445
Preprint. Discussion started: 26 March 2026

Ku	Ku-band radar
LCA	Rizoelia, Larnaca district radar
LWC	Liquid Water Content
MLP	Multilayer Perceptron
MS	Matched Scan
NN	Neural Network
PIA	Path Integrated Attenuation
PFO	Nata, Paphos district radar
PIR	Path-Integrated Reflectivity
QPE	Quantitative Precipitation Estimation
RBF	Radial Basis Function
RBFN	Radial Basis Function Network
RMSE	Root Mean Squared Error
SNR	Signal-to-Noise Ratio
SVR	Support Vector Regression
SRT	Surface Reference Technique
Z	Radar reflectivity factor
Z_H	Reflectivity at horizontal polarization
Z_V	Reflectivity at vertical polarization
Z_{DR}	Differential reflectivity
K_{DP}	Specific differential phase
Φ_{DP}	Total differential phase
V_H	Horizontal radial velocity
V_V	Vertical radial velocity
W_H	Horizontal spectral width of radial velocity
W_V	Vertical spectral width of radial velocity

1 Introduction

Polarimetric weather radars provide enhanced insights into precipitation characteristics by enabling the estimation of parameters such as the mean particle size, the hydrometeor type, and the drop shape. Nevertheless, the multiple sources of uncertainty that affect radar-based quantitative precipitation estimation (QPE), such as attenuation, beam blockage and calibration errors, pose significant challenges to reliable QPE in atmospheric sciences.

A fundamental approach for rainfall estimation from radar data is through the so-called Z–R relationships, which link the

https://doi.org/10.5194/egusphere-2026-445
Preprint. Discussion started: 26 March 2026

radar reflectivity factor Z to the rainfall rate R based on assumptions about the drop size distribution (DSD). For example, using the Marshall-Palmer exponential DSD (Marshall and Palmer, 1948), Z is proportional to the sixth moment of the drop size distribution, whereas the liquid water content (LWC) corresponds to the third moment. This allows empirical power-law relations between Z and LWC, and between Z and R, to be derived. For typical midlatitude rain, the relationships can be expressed in the general forms:

$$R = a_r Z^{b_r}, \tag{1}$$

$$W = cZ^d \tag{2}$$

where R is the rain rate (mm h^{-1}), W is the LWC (g m^{-3}), and a_r, b_r, c, and d are coefficients determined empirically from collocated radar and rain gauge data and that depend on environmental conditions, such as humidity and atmospheric characteristics (Atlas and Ulbrich, 1977). As a result, the Z–R relation is not universally valid, it must be determined empirically for specific meteorological regimes and often performs poorly when applied under different conditions to those it was derived from. These limitations of Z–R are particularly significant for X-band radars. X-band radars are cost effective radar systems that provide high spatial resolution, but are highly susceptible to attenuation and calibration errors. The Cyprus national precipitation radar network comprises two X-band radars, which lack routine calibration and attenuation correction procedures.

In recent years, machine learning (ML) methods have emerged as a promising alternative to traditional empirical methods for radar-based precipitation estimation (Peng et al., 2022; Osman and Tahir, 2023; Rosenhoover et al., 2025). Bringi and Chandrasekar (2001) distinguish between physical and statistical/engineering methods for the estimation of rainfall using radar data. Physical methods employ rain models to calculate the rain rate. Such models are based on the physical characteristics of the raindrop, such as its shape and size distribution. Statistical/engineering methods, on the other hand, take into account complementary information, e.g. rain gauge measurements, in estimating the rainfall rate. Machine learning techniques fall within the latter category and offer powerful tools for training models to estimate rainfall based on radar and complementary data.

Several studies have demonstrated the potential of neural networks (NN) in this domain (Tsintikidis et al., 1997; Bellerby et al., 2000; Christodoulou et al., 2004; Cheng et al., 2023). An earlier study by Xiao and Chandrasekar (1997) developed two three-layer perceptron neural networks; one involving as input only the horizontal reflectivity Z_H and the other involving both Z_H and the differential reflectivity ZDR. For the training of the networks, they used multiparameter radar and rain gauges data. Their findings suggested that training the NN with both Z_H and ZDR yields a more accurate rainfall estimation, compared to those trained only with Z_H. Xu and Chandrasekar (2005) trained an adaptive radial basis function network (RBFN) using solely rain gauges data, while Alqudah et al. (2013) applied a similar methodology, complementing it with a principal component analysis in order to reduce the dimensionality of the input dataset and consequently reduce overfitting. Teschl et al. (2007) employed a feedforward back-propagation neural network (BPNN) to estimate surface rainfall by learning the relationship between radar reflectivity profiles in the vertical column and rain gauge measurements. Inputs include the vertical profile of reflectivity and the maximum height of the detected precipitation. Because of a 5-minute average lag between radar observations and ground measurements, the network was trained to predict ground rainfall 5 minutes ahead. Orlandini and Morlini (2000) compared three artificial neural networks (ANNs), namely the multilayer perceptron (MLP), the Bayesian network (BN), and

https://doi.org/10.5194/egusphere-2026-445
Preprint. Discussion started: 26 March 2026

the RBFN. Their study yielded more accurate results for BN that achieved the lowest Root Mean Squared Error (RMSE) values and a more reliable prediction of rainfall peaks. They also found that the inclusion of additional input variables, such as the temporal variability of reflectivity, further improve the BN. On the contrary, MLP and RBFN resulted in worse performance, when more input variables were taken into consideration.

An important consideration in involving rain radar measurements and rain gauges for the training of neural networks is the radar sample resolution (both horizontal and vertical) above the rain gauge at which the reflectivity is measured. Li et al. (2003) derived best results at heights 1 km to 4 km above surface with 1 km horizontal resolution. The same resolution was also applied by Chen et al. (2019), who implemented a two-phase deep NN to first correlate the ground radar reflectivity with gauges rainfall intensity and then to derive rainfall at ground using spaceborne radar data.

More recent advancements proposed further sophisticated architectures, such as convolutional neural networks (CNNs) (Yang et al., 2019; Ayzel et al., 2020; Zhang et al., 2021; Caseri et al., 2022). In particular, Zhang et al. (2021) applied a one-dimensional CNN for the implementation of a real-time precipitation estimation framework. Their network involved not only radar reflectivity data, but also meteorological factors. Their validation was done based on a weather station network and resulted in improved results compared to traditional Z–R relationships and BPNNs. Confirming previous findings (Orlandini and Morlini, 2000), the inclusion of meteorological parameters improved the model's performance and enhanced the accuracy of the precipitation estimates.

Despite the above advances, major challenges persist, as many ML-based rainfall estimation methods rely on well-calibrated and attenuation-corrected radar data, which are often unavailable in the case of X-band radars. Additionally, ML-based rainfall retrieval methods rely often on ground references and approaches that are solely based on spaceborne radar measurements, which remain largely unexplored.

In this study, a two-stage, ML framework is proposed for the estimation of near-surface rainfall from ground-based X-band radar measurements over Cyprus. In the first stage, a feedforward NN is trained to correct ground radar reflectivity using volume-matched reflectivity observations from the Global Precipitation Measurement (GPM) Mission dual-frequency precipitation radar (DPR) Ku-band. In the second stage, the corrected reflectivity is used as input to regression models, including machine learning techniques, to estimate near-surface rainfall rates using measurements from automatic weather stations.

2 Data

This study is based on reflectivity data from the Ku-band radar onboard GPM mission's core satellite, as well as data from the two ground X-band dual polarization radars and from the network of Automatic Weather Stations (AWS) of the Cyprus Department of Meteorology. This Section provides the details of the datasets employed.

2.1 GPM DPR Ku-Band radar data (GPM_2AKu)

This study is based on reflectivity observations from the Ku-band radar of the Global Precipitation Measurement mission Dual-frequency Precipitation Radar (GPM DPR Ku, hereafter GPM Ku). The Ku-band performs Normal Scans (NS) with

https://doi.org/10.5194/egusphere-2026-445
Preprint. Discussion started: 26 March 2026

49 footprints, each with an approximate horizontal resolution of 5 km. In contrast, the Ka-band operates in two modes: the Matched Scan (MS), which includes 25 footprints aligned with the inner 25 Ku-band footprints, and the High Sensitivity Scan (HS), which consists of 24 footprints shifted by half a footprint relative to the MS configuration. The range resolution is 250 m for all scan modes except HS, which has a coarser resolution of 500 m. Similarly, the vertical resolution is 125 m for both Ku-band and Ka-band (MS), while Ka-band (HS) has a vertical resolution of 250 m. Starting from Level-2 version V06X, all GPM DPR products are provided in a Full Swath (FS) format. This FS structure corresponds to the Ku-band NS configuration, whereas the Ka-band FS dataset integrates both MS and HS observations (Iguchi et al., 2021).

Both Ku- and Ka-band radars are affected by signal attenuation, which can exceed 10 dB for the Ku-band. When attenuation is significant, the Surface Reference Technique (SRT) is applied to estimate the Path Integrated Attenuation (PIA). For weaker but still non-negligible attenuation, the Hitchfeld–Bordan (HB) method is used (Meneghini et al., 2015; Iguchi et al., 2021).

In this work, the vertical profiles of the reflectivity factor were derived from DSD estimates obtained from the Ku-band FS Level-2 product(file specification 2ADPR, (Iguchi et al., 2021)), specifically using the parameter zFactorFinal. This variable accounts for attenuation effects due to clouds, atmospheric gases, and precipitation (Meneghini et al., 2021).

2.2 Ground radar data

The Cyprus radar network comprises two ground X-band dual polarization radars operated by the Department of Meteorology of the Republic of Cyprus. The radar stations are located in Rizoelia, Larnaca district (LCA), and Nata, Paphos district (PFO). Technical information regarding the two X-band radars is given in Table 1. Both radars are installed on the top of hills.

Table 1. Technical description of the X-band radars.

Radar location	**Rizoelia, Larnaca district (LCA)**	**Nata, Pafos district (PFO)**
Beginning of operation	October 2017	January 2018
Latitude	34.94° N	34.77° N
Longitude	33.57° E	32.55° E
Altitude	100 m	392 m
Radar frequency	9.15 GHz	8.95 GHz
Signal processor	Enigma3+/Enigma4 dualpol	
Manufacturer	GAMIC GmbH	
Number of PPI scans	8	
Elevation angles (PPI)	0.5° to 30°	

https://doi.org/10.5194/egusphere-2026-445
Preprint. Discussion started: 26 March 2026

The LCA radar began operations in October 2017, followed by the PFO radar in January 2018. Both radar stations undergo maintenance breaks during the dry season (typically from May/June to September/October), when the radars are temporarily shutdown. During the study period, the radars had a range coverage of 150 km (Figure 1).

Both radars have an azimuthal resolution of 1° and scan in PPI mode, with eight (8) surveillance scans per volume scan. The lowest elevation angle is 0.5° and the highest 30°. Their range resolution fluctuates between 100 and 2600 m, depending on the specific scan configuration. The time needed for the completion of a whole volume scan is approximately 3 min. The time gap between each volume scan is not constant for LCA and PFO radars, but it varies between 5 and 10 min depending on the scanning operation.

The following polarimetric variables are provided in raw format for each of the eight PPI surveillance scans: reflectivity at horizontal polarization (Z_H), reflectivity at vertical polarization (Z_V), differential reflectivity (Z_{DR}), total differential phase (Φ_{DP}), specific differential phase (K_{DP}), horizontal/vertical radial velocity (V_H, V_V), horizontal/vertical signal-noise ratio (SNR_H, SNR_V), uncorrected horizontal/vertical reflectivity factor (UZ_H, UZ_V), and horizontal/vertical spectral width of radial velocity (W_H, W_V). Further details on the radar specifications are given in Ivanov et al. (2021).

2.3 Automatic Weather Station (AWS) data

This work employs rainfall measurements from 37 AWS of the Cyprus meteorological stations network (see Figure 1). In particular, this study considered rainfall data obtained from tipping bucket rain gauge stations (hereafter referred to as pulse data), which were provided in the form of timestamped event records. Each timestamp indicated the moment the bucket tipped, corresponding to a known, fixed rainfall depth (e.g., 0.2 mm). In order to be comparable to the reflectivity measurements, the pulse data were first converted from local to UTC time. To derive rainfall intensity in units of millimetres per hour (mm/h), a time-based conversion was applied. For each recorded event, the time difference from the previous tip was calculated and the instantaneous rainfall rate was then estimated as follows:

$$\text{Rainfall Rate (mm/h)} = \frac{\text{Tip Volume (mm)}}{\text{Time Difference (s)}} \times 3600 \tag{3}$$

Events with large time gaps (> 10 min) or resulting in implausibly high intensities (> 150 mm/h) were filtered out to avoid erroneous spikes due to errors or data gaps.

https://doi.org/10.5194/egusphere-2026-445
Preprint. Discussion started: 26 March 2026

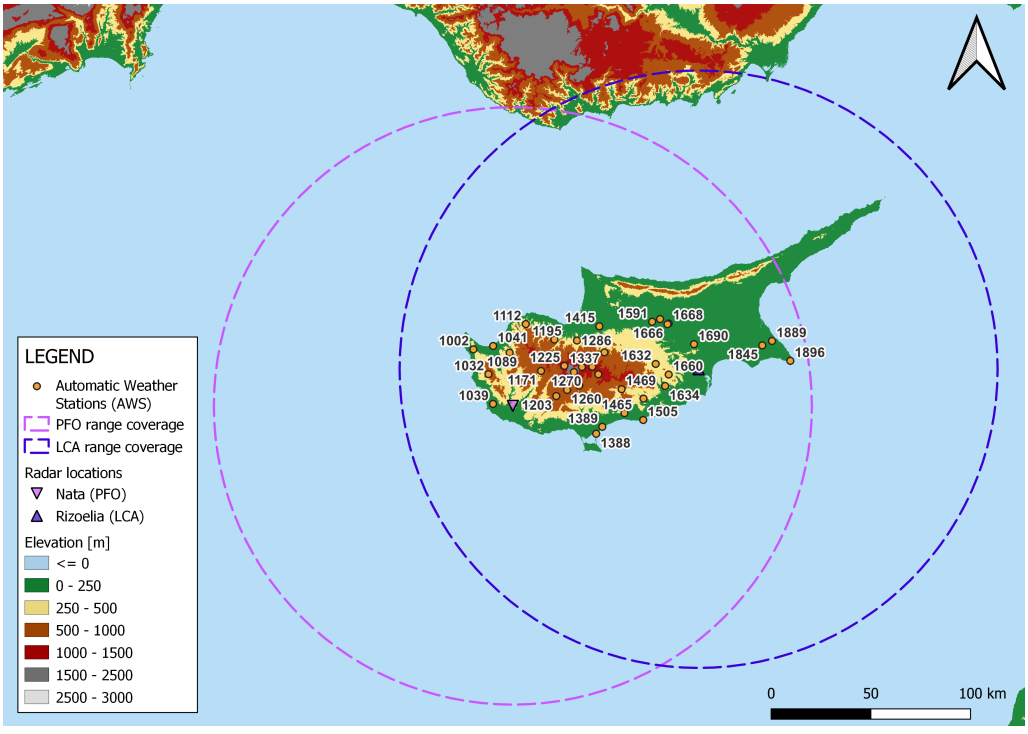

Figure 1. Geographical location of the 37 Automatic Weather Stations (AWS) with respect to the radar locations and their spatial coverage (i.e. 150 km).

2.4 Study period and data availability

The analysis focuses on the hydrological year from October 2019 to September 2020, which was identified by Loulli et al. (2025a) as a stable calibration period for both ground-based X-band radars. During this period, both radars were operational and provided continuous observations, subject to routine maintenance interruptions. GPM DPR overpasses and AWS rainfall measurements were available for the same temporal window and were used in the subsequent analysis.

3 Methodology

This study involved a two-stage framework to convert ground radar reflectivity measurements into near-surface rainfall rates. This framework was applied separately for each stable calibration period identified in the previous step and was divided into two sequential learning tasks:

- **Stage 1**: A feedforward NN that corrects the ground radar reflectivity using GPM Ku volume-matched reflectivity.
- **Stage 2**: A regression modelling stage in which near-surface rainfall rates are estimated using the corrected ground reflectivity using pulse data.

https://doi.org/10.5194/egusphere-2026-445
Preprint. Discussion started: 26 March 2026

The initial step for the development of the network was to define the input and output vectors. The input vector of the first network (Stage 1) consisted of four variables:

- the volume-matched raw ground reflectivity,
- the corresponding range to the ground radar,
- the corresponding Path-Integrated Reflectivity (PIR), and
- the GPM overpass time.

PIR was calculated as follows:

$$PIR_i = 10 \cdot \log_{10}\left(10^{\frac{Z_i}{10}} \cdot \Delta r_i\right) \tag{4}$$

where, Z_i is the reflectivity factor (in dBZ) at a volume-matched sample i and Δr_i (m) is its range to the ground radar. The output vector consisted of one variable, namely the volume-matched GPM Ku reflectivity.

The output of the first network, i.e., the corrected ground reflectivity, was then used as an input variable in data-driven models that estimate near-surface rainfall rates from the corrected ground reflectivity using pulse data. Particularly, Linear Regression, Support Vector Regression (SVR), a feedforward NN, and Random Forest were initially tested. As SVR and the feedforward NN exhibited better performance, they were chosen to be further used in this work.

Before proceeding to the second stage, a preliminary analysis was done using the corrected reflectivity data. Specifically, rainfall rates were estimated using two empirical Z–R relationships, employing the corrected reflectivity at the nearest radar gate to each pulse station, as well as the spatially averaged reflectivity over circular areas with radii of 100, 250, 500, and 800 m centered on the pulse station location. In this procedure, only the lowest radar sweep was considered. The correlation between the Z–R-derived and pulse-derived rainfall rates was then calculated for each Z–R relationship and spatial scale. The spatial scale that resulted in the highest correlation was selected to be subsequently used in the training of the second neural network. The following Z–R relationships, which are based on the Marshall-Palmer relation (Marshall and Palmer, 1948), were used:

- Z–R relationship applied by Tartaglione et al. (2008) (hereafter denoted as TGM08)

$$Z = 316R^{1.5} \tag{5}$$

- a power-law-fitted Z–R relationship, following Equation (1) (hereafter denoted as fZR).

Equations (5) was adopted for the Cyprus context and particularly for the Kykkos C-band radar data conversion into rainfall rates. In both equations (5) and (1), Z denotes the radar reflectivity factor in $\mathrm{mm^6\,m^{-3}}$, and R denotes the rainfall rate in mm/h. To construct the training vectors for the second-stage data driven models, the closest-in-time radar volume scan was identified for each pulse record, within a $\pm$10-min window. Additionally, the time difference between the radar volume scan and the pulse tip was estimated. To assess how the time difference between the radar scan and the pulse tip affected their agreement, a sensitivity analysis using the above-explained Z–R relationships was performed. The time difference range that yielded more

https://doi.org/10.5194/egusphere-2026-445
Preprint. Discussion started: 26 March 2026

reliable performance metrics was identified; pulse data recorded at higher time differences were excluded from the training process. Following the afore-explained procedure, the input vector of the data-driven models included two variables:

- the corrected ground reflectivity at the selected spatial scale, and
- the time difference between the radar volume scan and the pulse tip.

The output vector comprised one variable, namely the pulse-derived rainfall rate.

The above-described methodology was applied for each ground radar separately and the performance metrics of the data-driven models were compared with those of the traditional Z–R algorithms metrics. A diagram illustrating the full processing pipeline is shown in Figure 2. The following subsections present the procedure and the model architecture for each radar individually, followed by a description of the performance evaluation metrics.

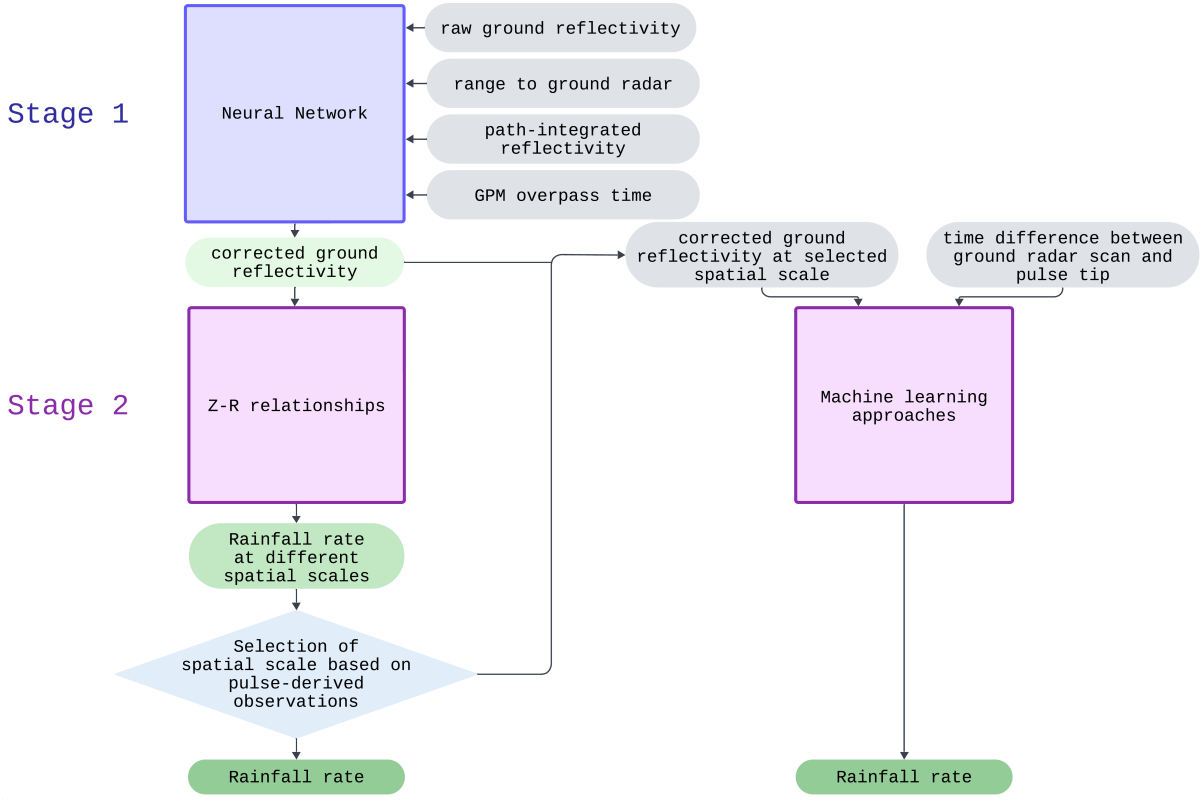

Figure 2. Overview of the processing pipeline for the rainfall rate retrieval.

https://doi.org/10.5194/egusphere-2026-445
Preprint. Discussion started: 26 March 2026

3.1 Rainfall rate estimation framework for LCA radar

3.1.1 Stage 1: Reflectivity Correction

The dataset used for the feedforward NN for LCA radar (Stage 1) was first split into training (80%), validation (9%) and test (11%) sets, followed by a normalization to scale the input variables between 0 and 1. The model architecture was a four-layer perceptron network, consisting of an input layer with 4 nodes, followed by 3 hidden layers with 512, 16 and 4 ReLU-activated neurons, respectively. The output layer comprised a single neuron with exponential activation function. The model was trained using the Adam optimizer (learning rate = 0.001) and Mean Absolute Error (MAE) as the loss function. The training of the network was performed over 2000 epochs with a batch size of 64.

3.1.2 Stage 2: Rainfall Rate Estimation

The dataset used for the feedforward NN for LCA radar (Stage 2) was first split into training (80%), validation (10%) and test (10%) sets, followed by a normalization to scale the input variables between 0 and 1. The model architecture was a four-layer perceptron network, consisting of an input layer with 2 nodes, followed by 3 hidden layers with 16, 8 and 4 ReLU-activated neurons, respectively. The output layer comprised a single neuron with linear activation function. The model was trained using the Adam optimizer (learning rate = 0.005) and MAE as the loss function. The training of the network was performed over 30 epochs with a batch size of 32.

The SVR model developed for the LCA radar (Stage 2) followed a similar preprocessing as the neural network model. The dataset was first split into training (80%), validation (10%), and test (10%) sets and the input variables were normalized. A regression pipeline was constructed using a Radial Basis Function (RBF) kernel SVR model, while the maximum number of iterations for the SVR solver was set to 900. To optimize the SVR configuration using 3-fold cross-validation, a grid search over a predefined hyperparameter space was employed. Due to its highly skewed distribution, the pulse-derived rainfall rate was log-transformed using the $\log(1 + R)$ transformation during training. Model predictions on the test set were subsequently inverse-transformed for final evaluation and comparison with pulse-derived rainfall rates.

3.2 Rainfall rate estimation framework for PFO radar

3.2.1 Stage 1: Reflectivity Correction

The dataset used for the feedforward NN for PFO radar (Stage 1) was first split into training (80%), validation (10%) and test (10%) sets, followed by a normalization to scale the input variables between 0 and 1. The model architecture was a seven-layer perceptron network, consisting of an input layer with 4 nodes, followed by 6 hidden layers with 256, 128, 64, 16, 8 and 4 ReLU-activated neurons, respectively. The output layer comprised a single neuron with exponential activation function. The model was trained using the Adam optimizer (learning rate = 0.01) and MAE as the loss function. The training of the network was performed over 300 epochs with a batch size of 128.

https://doi.org/10.5194/egusphere-2026-445
Preprint. Discussion started: 26 March 2026

3.2.2 Stage 2: Rainfall Rate Estimation

The dataset used for the feedforward NN for PFO radar (Stage 2) was first split into training (80%), validation (10%) and test (10%) sets, followed by a normalization to scale the input variables between 0 and 1. The model architecture was a five-layer perceptron network, consisting of an input layer with 2 nodes, followed by 4 hidden layers with 32, 16, 4 and 2 ReLU-activated neurons, respectively. The output layer comprised a single neuron with linear activation function. The model was trained using the Adam optimizer (learning rate = 0.005) and MAE as the loss function. The training of the network was performed over 100 epochs with a batch size of 64.

The SVR model developed for the PFO radar (Stage 2) followed a similar preprocessing as the neural network model. The dataset was first split into training (80%), validation (9%), and test (11%) sets and the input variables were normalized. A regression pipeline was constructed using a RBF kernel SVR model, while the maximum number of iterations for the SVR solver was set to 900. To optimize the SVR configuration using 3-fold cross-validation, a grid search over a predefined hyperparameter space was employed. Due to its highly skewed distribution, the pulse-derived rainfall rate was log-transformed using the $\log(1+R)$ transformation during training. Model predictions on the test set were subsequently inverse-transformed for final evaluation and comparison with pulse-derived rainfall rates.

3.3 Performance evaluation

All machine learning models described above were evaluated using the following performance metrics:

- the Mean Absolute Error (MAE):

$$\text{MAE} = \frac{1}{n}\sum_{i=1}^{n}|y_i - \hat{y}_i|\,, \tag{6}$$

- the Root Mean Squared Error (RMSE):

$$\text{RMSE} = \sqrt{\frac{1}{n}\sum_{i=1}^{n}(y_i - \hat{y}_i)^2} \tag{7}$$

- the Mean Bias:

$$\text{Mean Bias} = \frac{1}{n}\sum_{i=1}^{n}(y_i - \hat{y}_i)\,, \tag{8}$$

- the Coefficient of Determination (r^2):

$$r^2 = 1 - \frac{\sum_{i=1}^{n}(y_i - \hat{y}_i)^2}{\sum_{i=1}^{n}(y_i - \bar{y})^2} \tag{9}$$

where, y_i, $\hat{y}_i$ and n denote the actual values, the predicted values, and is the number of sample points, respectively.

https://doi.org/10.5194/egusphere-2026-445
Preprint. Discussion started: 26 March 2026

4 Results

This section presents the results of the conversion of reflectivity measurements to near-surface rainfall rates, using a two-stage approach for reflectivity correction and rainfall estimation. The results are presented in two sections. Section 4.1 analyses the application of the two-stage framework to the LCA radar, which Section 4.2 details its implementation for the PFO radar.

4.1 Two-stage framework for LCA radar

For LCA radar, the first stage of the framework involved the training of a four-layer perceptron network. The network's performance metrics across the training, validation and test sets are shown in Table 2. With regard to the training set, the network achieved a MAE of 2.45 dBZ, a RMSE of 3.37 dBZ, a bias of 0.03 dBZ, with an r^2 of 0.73, indicating a good to strong fit. The network's performance remained consistent across validation and test sets with an r^2 of 0.68 in both cases, as well as low mean bias (± 0.3 dBZ or less).

Table 2. Performance metrics of the four-layer perceptron network across training, validation, and testing sets for LCA radar.

Set	MAE [dBZ]	RMSE [dBZ]	Mean bias [dBZ]	r^2
Train	2.45	3.37	0.03	0.73
Validation	2.47	3.31	0.30	0.68
Test	2.78	3.80	-0.09	0.68

The scatter plots in Figure 3 show the corrected LCA radar reflectivity estimates [dBZ] produced by the NN against GPM Ku reflectivity for the training and test sets. In both cases, the scatterers were well distributed along the 1:1 reference line, indicating a reliable correction of the ground reflectivity estimates. A slight tendency toward underestimation was observed, particularly in higher reflectivity ranges, but the overall agreement remained acceptable across the majority of observations.

https://doi.org/10.5194/egusphere-2026-445
Preprint. Discussion started: 26 March 2026

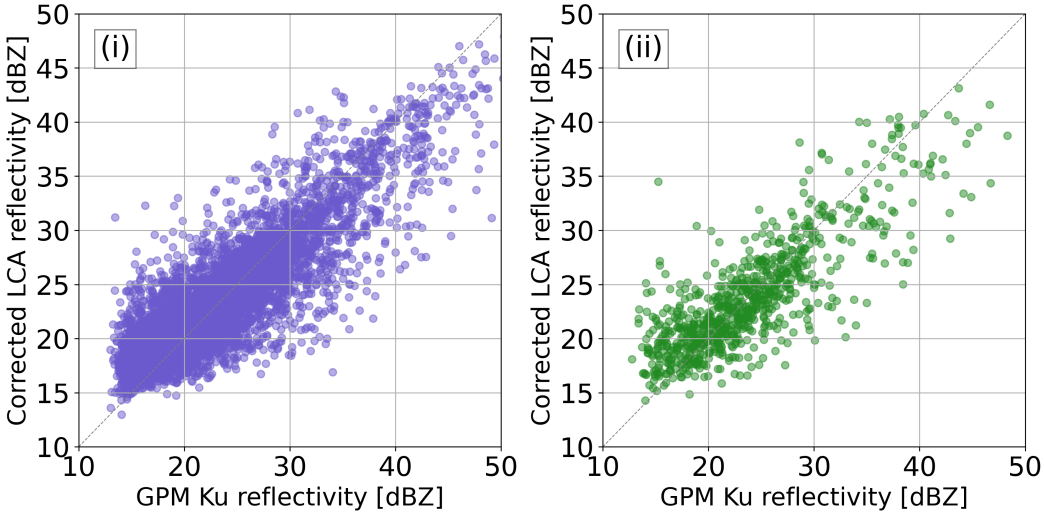

Figure 3. Scatter plots of corrected LCA radar reflectivity estimates [dBZ] produced by the four-layer perceptron network and GPM Ku reflectivity [dBZ]. (i) corresponds to the training dataset and (ii) corresponds to the test set.

Using the corrected LCA reflectivity from Stage 1 and testing how the time difference between radar scans and pulse tips affected a preliminary rainfall estimation performance, a time difference threshold of 7 min (where pulse tips were ahead of the radar) was chosen. With regard to the selection of the optimal spatial radius around each pulse station, a 100 m radius resulted in more reliable rainfall estimates, and was, therefore, adopted for the training of the second stage models for LCA radar.

Table 3 summarizes the performance metric of the results for the LCA radar Stage 2 data-driven models. As shown, the traditional $Z–R$ approaches (i.e., TGM08 and fZR) failed to produce reliable rainfall estimates. In particular, the fZR method resulted in extremely high inaccuracies and a strongly negative r^2, indicating a significant discrepancy between estimated and pulse-derived rainfall rates. On the contrary, the SVR model resulted in more acceptable estimates, with a MAE of 0.33 mm/h, a RMSE of 0.41 mm/h, a mean bias of 0.10 mm/h. However, its r^2 was calculated to be 0.27. The NN is presented separately for the training, validation and test sets. Despite the fact that the training and validation sets yielded considerable MAE (approximately 2-4 mm/h), RMSE (9-10 mm/h) and negative mean biases (-3- -2 mm/h), the model resulted in a noteworthy improvement on the test set, reaching a MAE of 1.39 mm/h, a RMSE of 2.32 mm/h, and a mean bias of –0.26 mm/h, along with an r^2 of 0.23.

https://doi.org/10.5194/egusphere-2026-445
Preprint. Discussion started: 26 March 2026

Table 3. Performance metrics (MAE, RMSE, Bias, r^2) for traditional Z–R methods and data-driven models for LCA radar. NN results are shown separately for training, validation, and test sets.

Model	Set	MAE [mm/h]	RMSE [mm/h]	Mean bias [mm/h]	r^2
TGM08	Full	4.54	9.92	-4.54	-0.26
fZR	Full	19.35	125.74	12.94	-201.42
SVR	Full	0.33	0.41	0.10	0.27
NN	Train	2.86	9.14	-1.97	-0.01
	Validation	3.38	10.32	-2.59	0.02
	Test	1.39	2.32	-0.26	0.23

The figures presented below visually support the performance metrics for the LCA radar. Figure 4 presents scatter plots comparing predicted rainfall rates [mm/h] from SVR and NN models against pulse-derived rainfall rates for the training and test sets. A consistent tendency toward underestimation was observed for both models. Notably, focusing on the range between 0–30 mm/h (see Appendix, Figure A1), the NN failed to predict rainfall rates above approximately 5 mm/h across both sets, highlighting a limitation in predicting higher rainfall intensities. The SVR model was able to produce rainfall estimates up to approximately 7.5 mm/h, which remain largely underestimated compared to the pulse-derived rainfall rates, as well. The overall trend in both models reflected a systematic underestimation, especially for rainfall rates higher than 5 mm/h.

Figure 5 illustrates pulse-derived precipitation rates with estimates from the fZR and the TGM08 algorithms. The results of both approaches were evidently unsatisfactory. The fZR method significantly overestimated the rainfall rate, producing much higher estimates than the pulse data, especially at low pulse rainfall rates. The TGM08 relationship performed poorly as well, producing values constrained within the narrow range of 0–1.25 mm/h, ignoring the variability in the pulse-derived rainfall (see Appendix, Figure A3). Fitting the Z–R relationship using the corrected reflectivity from LCA radar and the pulse-derived data yielded the parameters $a = 4.83$ and $b = 0.56$.

https://doi.org/10.5194/egusphere-2026-445
Preprint. Discussion started: 26 March 2026

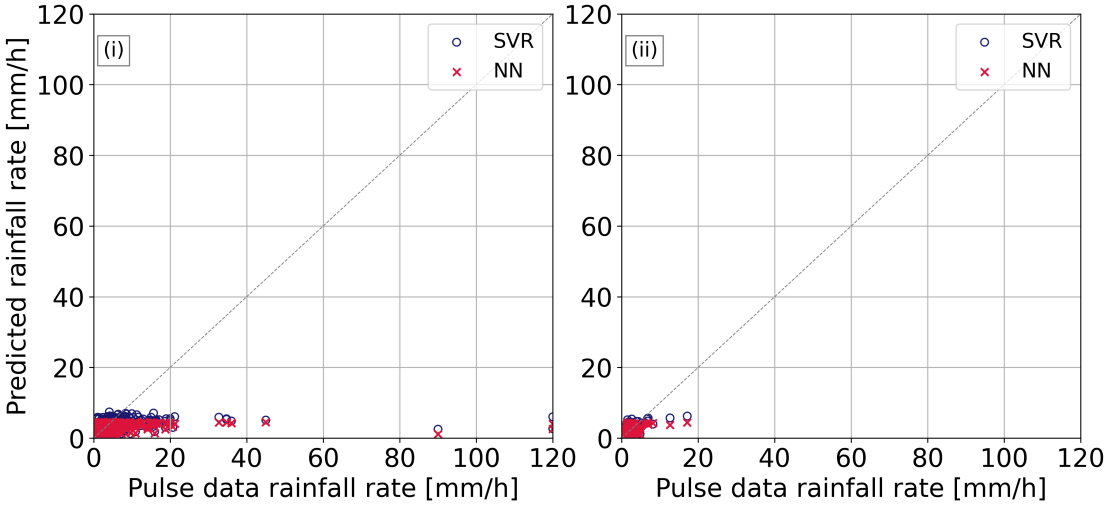

Figure 4. Scatter plots comparing predicted rainfall rate [mm/h] from SVR and NN models against pulse data rainfall rate [mm/h] for LCA radar. (i) corresponds to the training dataset and (ii) corresponds to the test set.

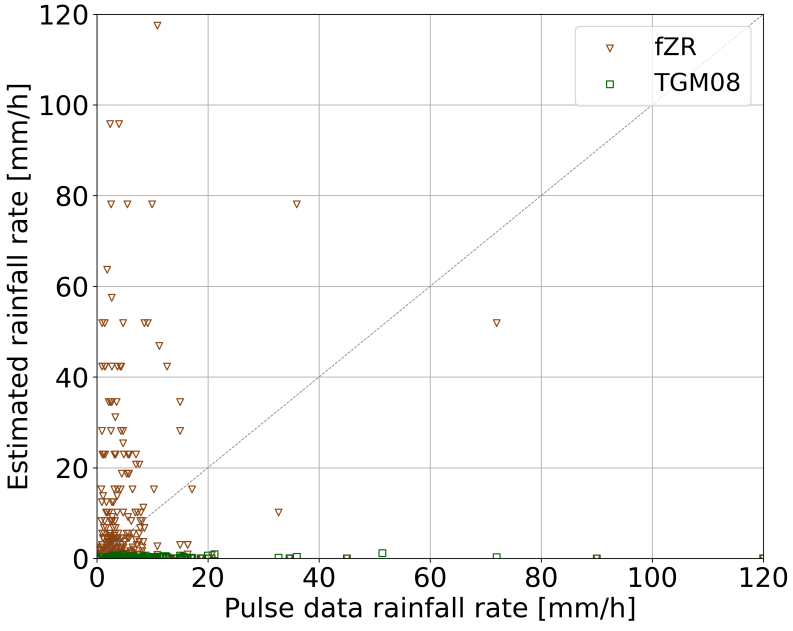

Figure 5. Scatter plot comparing pulse data rainfall rate [mm/h] with estimated rainfall rates from two methods: a fZR relationship (in brown) and the TGM08 relationship (in green) for LCA radar.

Despite the limitations observed in the performance of all models, the SVR approach demonstrated relatively more stable and interpretable behavior, particularly in capturing the broader range of rainfall intensities. Although moderate, these comparative

https://doi.org/10.5194/egusphere-2026-445
Preprint. Discussion started: 26 March 2026

advantage led to the selection of the SVR model for further application in rainfall mapping. Figure 6 illustrates indicative rainfall rates derived from the two-stage framework for LCA radar for the precipitation event of 12 December 2019. The rainfall rates were estimated using an interpolated time difference between the pulse station and the radar coverage area, which served as a proxy input for the SVR model.

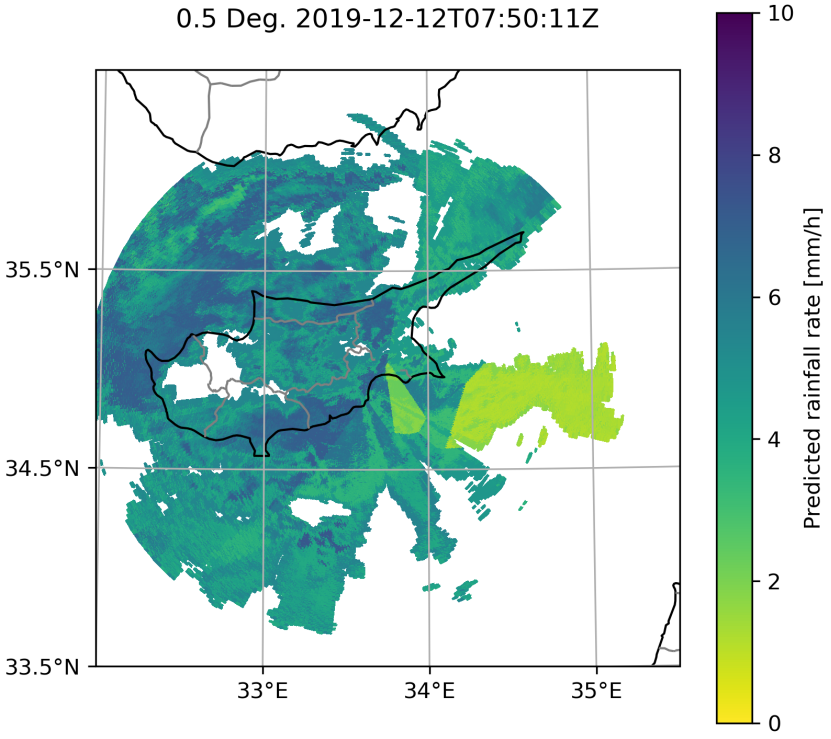

Figure 6. Predicted rainfall rate [mm/h] using the two-stage framework for LCA radar, for the precipitation event of 12 December 2019 (07:50:11 UTC) at 0.5° elevation angle.

4.2 Two-stage framework for PFO radar

For PFO radar, the first stage of the framework involved the training of a seven-layer perceptron network. The network's performance metrics across the training, validation and test sets are shown in Table 4. With regard to the training set, the network yielded a MAE of 3.19 dBZ, a RMSE of 4.32 dBZ, a mean bias of -0.07 dBZ, with an r^2 of 0.57, showing a moderate to acceptable fit. MAE and RMSE resulted in a minor increase across the validation and test sets, while r^2 decreased to 0.5 for validation and 0.53 for test set. In terms of bias, this network showed a consistent slight underestimation across all sets, with mean bias values ranging from -0.07 to 0.23 dBZ.

https://doi.org/10.5194/egusphere-2026-445
Preprint. Discussion started: 26 March 2026

Table 4. Performance metrics of the seven-layer perceptron network across training, validation, and testing sets for PFO radar.

Set	MAE [dBZ]	RMSE [dBZ]	Mean bias [dBZ]	r^2
Train	3.19	4.32	-0.07	0.57
Validation	3.47	4.58	-0.23	0.50
Test	3.29	4.32	-0.15	0.53

Figure 7 illustrates the scatterplots of the corrected PFO radar reflectivity estimates [dBZ] produced by theNNagainst GPM Ku reflectivity for the training and test sets. Similar to LCA radar, the scatterers were in both cases acceptably distributed along the 1:1 reference line, while there was a tendency for underestimation, particularly in higher reflectivity ranges. However, it is worth noting that the network for PFO radar exhibited difficulty correcting ground reflectivity values below 15 dBZ.

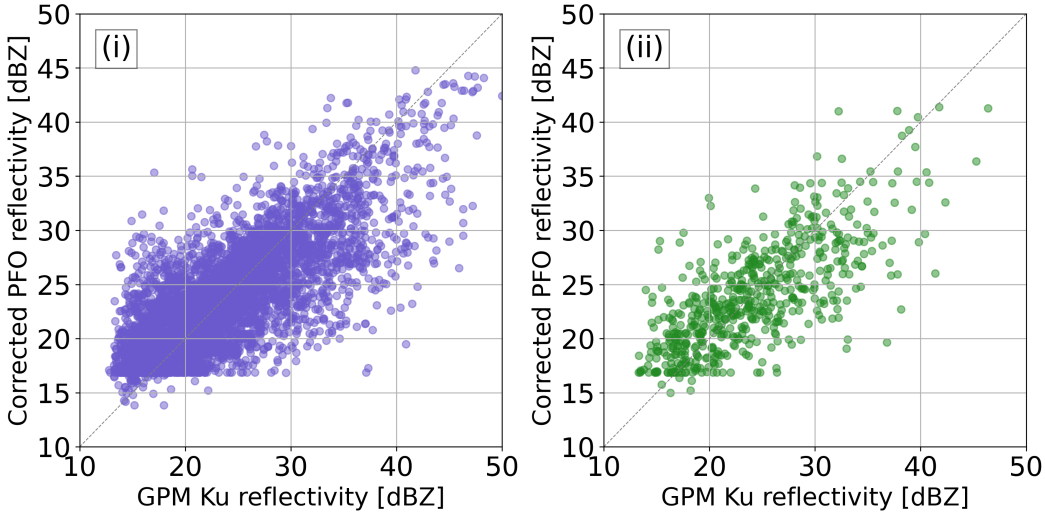

Figure 7. Scatter plots of corrected PFO radar reflectivity estimates [dBZ] produced by the seven-layer perceptron network and GPM Ku reflectivity [dBZ]. (i) corresponds to the training dataset and (ii) corresponds to the test set.

Similar to the procedure applied for the LCA radar, a preliminary evaluation of rainfall estimation performance was performed for the PFO radar, a 7 min time difference threshold (pulse tips ahead of radar) was also selected for the PFO radar, as well. With regard to the selection of the optimal spatial radius around each pulse station, the analysis showed that a 250 m radius provided more reliable rainfall estimates. Thus, this spatial scale was adopted for the training of the second stage models for PFO radar.

Table 5 presents the performance metrics for the Stage 2 models applied to the PFO radar. Similar to LCA, the traditional Z–R approaches (TGM08 and the fZR relationship) failed to provide reliable rainfall estimates. Notably, the fZR resulted in extremely large errors and an r^2 of –67.66, indicating a critical discrepancy between estimated and observed rainfall. The SVR

https://doi.org/10.5194/egusphere-2026-445
Preprint. Discussion started: 26 March 2026

model yielded moderate improvement, achieving an MAE of 0.53 mm/h and a RMSE of 0.76 mm/h, with a small negative bias (–0.09 mm/h), though its r^2 remained low at 0.078. The neural network, evaluated separately across training, validation, and test sets, exhibited inadequate performance. Its training and validation sets yielded a MAE of 3–4 mm/h and a RMSE of 7–9 mm/h, with negative mean biases of approximately -1 mm/h. The test set performance resulted in lower performance, with a MAE of 4.61 mm/h, a RMSE of 14.06 mm/h, and a mean bias of –2.94 mm/h. The test set r^2 decreased to –0.03.

Table 5. Performance metrics (MAE, RMSE, Bias, r^2) for traditional Z–R methods and data-driven models for PFO radar. NN results are shown separately for training, validation, and test sets.

Model	Set	MAE [mm/h]	RMSE [mm/h]	Mean bias [mm/h]	r^2
TGM08	Full	5.55	11.07	-5.54	-0.32
fZR	Full	14.40	91.20	7.34	-67.66
SVR	Full	0.53	0.76	-0.09	0.078
NN	Train	3.44	8.89	-1.97	0.07
	Validation	3.35	7.10	-1.92	0.06
	Test	4.57	14.06	-2.94	-0.03

The figures presented below visually reinforce the evaluated performance metrics of the PFO radar. Figure 8 shows scatter plots comparing predicted rainfall rates [mm/h] from the SVR and NN models against pulse-derived rainfall rates for both the training and test sets. Similar to the models for LCA, both models exhibited a consistent underestimation tendency. The SVR model produced rainfall rates up to approximately 65 mm/h in the training set, yet in the test set it only reached up to about 30 mm/h, with only one prediction, which was a significant overestimation. On the other hand, the neural network failed to predict rainfall rates below approximately 1.5 mm/h (see Appendix, Figure A2), indicating limited sensitivity to light rainfall events. In contrast, the SVR model was able to produce low-intensity predictions.

Figure 9 compares pulse-derived rainfall rates with estimates from two Z–R relationships. Both methods delivered considerably poor results. Similar to LCA radar, the fZR approach yielded estimates that overestimate the near-surface rainfall rate, while the TGM08 relationship performed weakly as well, providing values strictly within the 0–3 mm/h range (see Appendix, Figure A4). Fitting the Z–R relationship using the corrected reflectivity from PFO radar and the pulse-derived data yielded the parameters $a = 6.08$ and $b = 0.81$.

https://doi.org/10.5194/egusphere-2026-445
Preprint. Discussion started: 26 March 2026

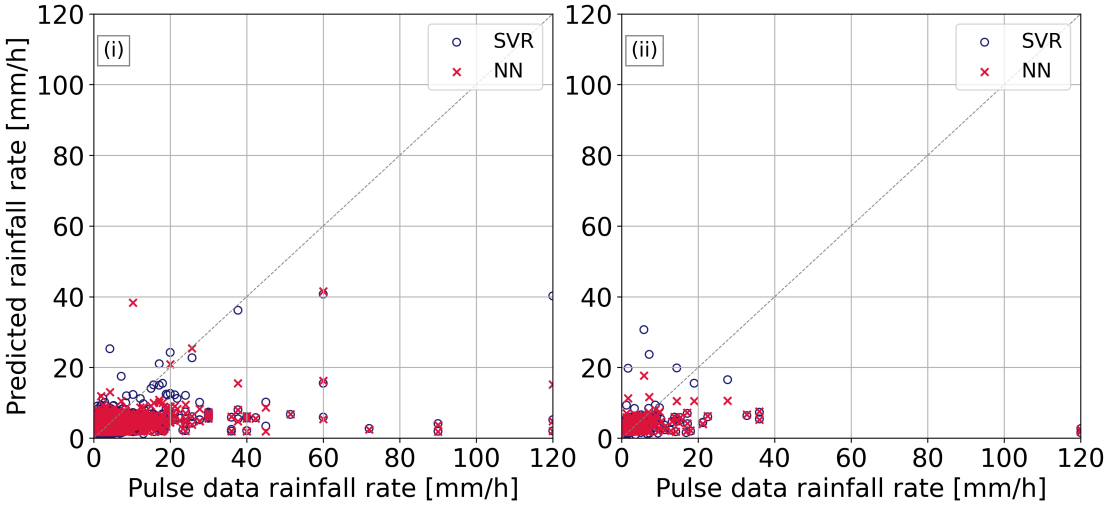

Figure 8. Scatter plots comparing predicted rainfall rate [mm/h] from SVR and NN models against pulse data rainfall rate [mm/h] for PFO radar. (i) corresponds to the training dataset and (ii) corresponds to the test set.

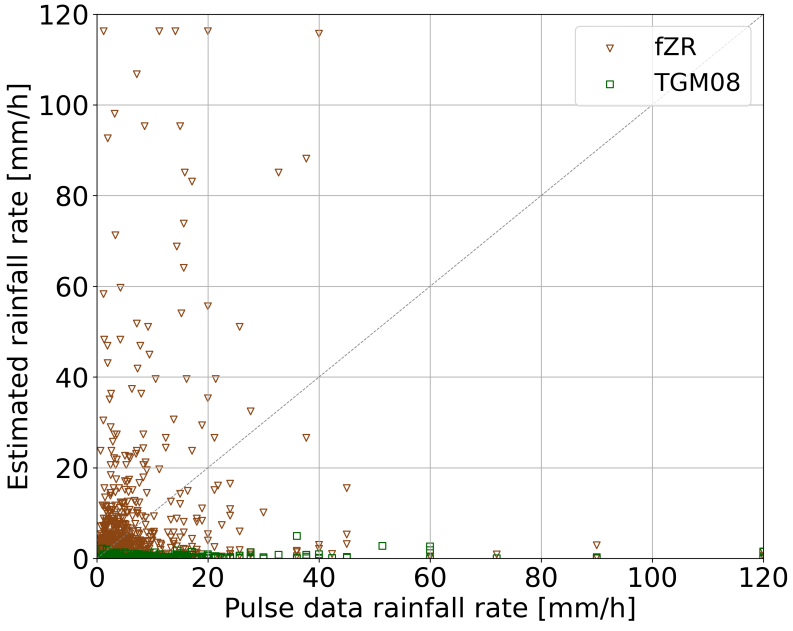

Figure 9. Scatter plot comparing pulse data rainfall rate [mm/h] with estimated rainfall rates from two methods: a fZR relationship (in brown) and the TGM08 relationship (in green) for PFO radar.

320 Similar to the LCA radar, the SVR model for the PFO radar exhibited comparatively better consistency than the alternative models. Despite its overall limited accuracy, its relative advantages supported its selection for subsequent rainfall mapping

https://doi.org/10.5194/egusphere-2026-445
Preprint. Discussion started: 26 March 2026

applications. Figure 10 presents indicative rainfall estimates by the two-stage framework for the PFO radar, corresponding to the 12 December 2019 event. Similar to LCA radar, rainfall rates were estimated using an interpolated time difference as a proxy input to the SVR model.

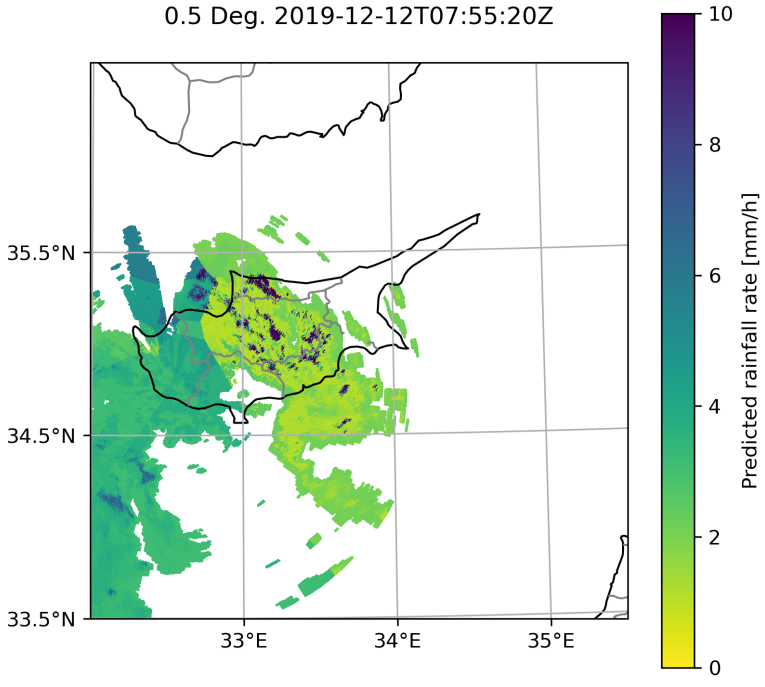

Figure 10. Predicted rainfall rate [mm/h] using the two-stage framework for PFO radar, for the precipitation event of 12 December 2019 (07:55:20 UTC) at 0.5° elevation angle.

Figure 11 illustrates the predicted rainfall rates from LCA and PFO radars mapped on a cartesian grid. This mapping was performed for altitudes ranging from 500 m to 4 km, with a horizontal resolution of 1 km.

https://doi.org/10.5194/egusphere-2026-445
Preprint. Discussion started: 26 March 2026

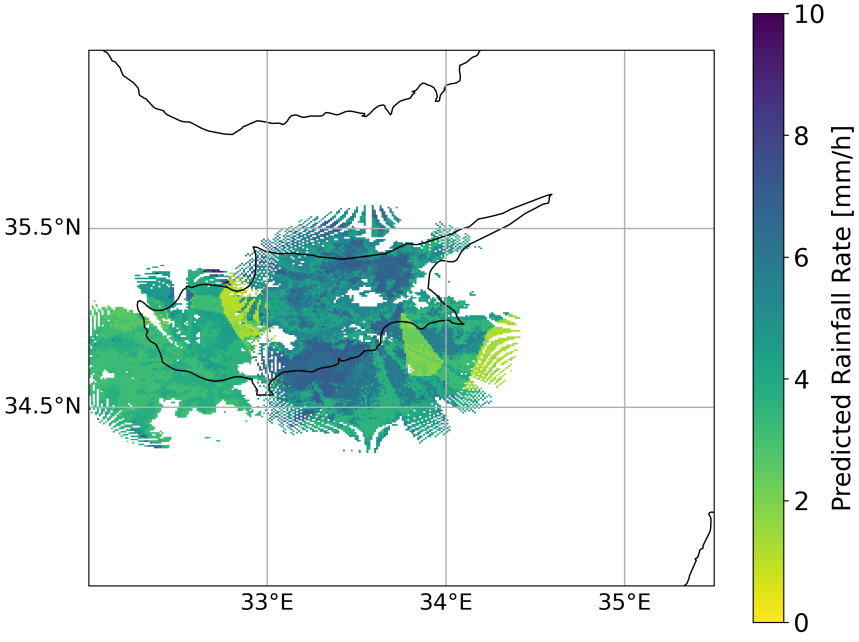

Figure 11. Merged predicted rainfall rate [mm/h] using the two-stage framework, combining PFO radar (07:55:20 UTC) and LCA radar (07:50:11 UTC) observations at 0.5° elevation angle for the precipitation event of 12 December 2019.

5 Discussion

The analysis of the two-stage framework for converting ground radar reflectivity to near-surface rainfall rates revealed several important insights. One important finding concerns the optimal spatial radius around each pulse station used to average the radar reflectivity data for training the second stage models. For the LCA radar, a 100 m radius was found to provide the most reliable rainfall estimates, whereas for the PFO radar, a larger radius of 250 m was optimal. This difference may be attributed to the higher altitude of the PFO radar, which likely influences the spatial representativeness of the radar reflectivity at ground level. Interestingly, despite the altitude difference, the same optimal time difference of 7 min between the radar volume scan and the pulse measurement for training was derived for the training of both radars. This suggests that factors other than altitude, such as atmospheric dynamics, may influence the temporal matching window.

In terms of model complexity and performance, the PFO radar required a deeper NN architecture in both stages, yet it consistently yielded poorer results compared to the LCA radar. This difference may reflect challenges related to the PFO radar location, configuration, or data quality.

Moreover, traditional empirical Z–R relationships were found to be unable to reliably estimate the rainfall rate estimation in this context and are thus not suggested for further consideration. In contrast, machine learning methods demonstrated promising results, showing improved flexibility and predictive skill in predicting the rainfall rate using ground radar reflectivity measurements.

https://doi.org/10.5194/egusphere-2026-445
Preprint. Discussion started: 26 March 2026

The first stage of the two-stage framework, which focused on correcting ground radar reflectivity using volume-matched GPM Ku data, demonstrated effective results. This first stage significantly improved the quality of ground radar reflectivity inputs, and could potentially serve as an alternative or complementary approach to the attenuation correction and calibration methods for the Cyprus radar network.

However, the second stage, which estimated rainfall rates from the corrected reflectivity using pulse data, faced major limitations with regard to its input data. The substantially underestimated rainfall rates observed in the outputs of the NN, SVR, and the TGM08 relationship may also originate from the fact that the corrected reflectivity values remained somewhat underestimated. This residual underestimation in reflectivity is inherently continued into the rainfall rate estimations, embedding an additional layer of uncertainty that these models inherit and propagate.

Additionally, the pulse-derived rainfall rates themselves are not direct measurements but rather conversions from rainfall height records recorded at tipping bucket weather stations. This intrinsic inaccuracy in the input data possibly introduced uncertainty into the training of the models and ultimately affected their performance. The estimated rainfall fields exhibited also a strong dependence on the distance to the tipping bucket stations, because the SVR model relied on the interpolated time difference as a proxy input. This limitation was also evident in the resulting rainfall maps. However, when the predicted rainfall rates from the two ground radars were mapped together onto a common grid, the discrepancies between the rainfall estimates decreased considerably. This suggests that the spatial alignment of the two datasets helped mitigate some of the individual model uncertainties, leading to a more coherent rainfall distribution. Attempts to train the SVR using only the corrected reflectivity values, without incorporating the proxy variable, resulted in significantly poorer predictions.

Existing research on radar reflectivity–rainfall conversion using machine learning methods predominantly relies on rain gauge observations for model training (Liu et al., 2024; Huangfu et al., 2024; Rosenhoover et al., 2025). The present study builds on this research area by incorporating spaceborne GPM Ku-band radar observations in addition to rain gauge data. The integration of satellite radar measurements in Stage 1 of the two-stage framework provided a more consistent and independently constrained reflectivity dataset for the subsequent rainfall estimation in Stage 2. As discussed above, the NN-based correction applied in Stage 1 reduced systematic biases in the ground radar reflectivity and improved the quality of the inputs used by the Stage 2 rainfall estimation models.

6 Conclusions

A two-stage framework was investigated for radar-based quantitative precipitation estimation over Cyprus. Its Stage 1 NNs improved the ground radar reflectivity accuracy, demonstrating applicability in contexts, where conventional attenuation calibration correction approaches, previously examined in this radar network (attenuation correction in Loulli et al. (2025b), calibration correction in Loulli et al. (2025a)) are limited or unavailable. The Stage 2 models indicate that traditional Z–R methods are not optimal for the calculation of radar-based rainfall rates in Cyprus, and suggest further exploration of machine learning methods (particularly SVR models).

https://doi.org/10.5194/egusphere-2026-445
Preprint. Discussion started: 26 March 2026

Challenges in rainfall estimation using records from the Cyprus radar network remain, particularly regarding the quality of the pulse-derived rainfall rates, which are indirectly derived from tipping bucket records. This significant input uncertainty likely affected the overall performance of the Stage 2 models. Given that the discrepancies between the rainfall estimates from LCA and PFO decreased considerably when mapped together onto a common grid, future work should explore the application of the two-stage framework using both ground radars jointly mapped onto a common grid. This approach may enhance consistency and improve the overall rainfall estimation accuracy.

Despite remaining uncertainties, this study provides fundamental insights for QPE in Cyprus, offering a practical reference for researchers operating X-band radars with limited dual-frequency capabilities and informing the development of improved radar-based rainfall estimation methods.

Data availability. The ground radar data, as well as the AWS data, are available upon request from the Cyprus Department of Meteorology, subject to their data-sharing policy. The GPM data are publicly accessible and were obtained from the NASA Earthdata portal (https://search.earthdata.nasa.gov/, accessed on 18 April 2023).

Appendix A

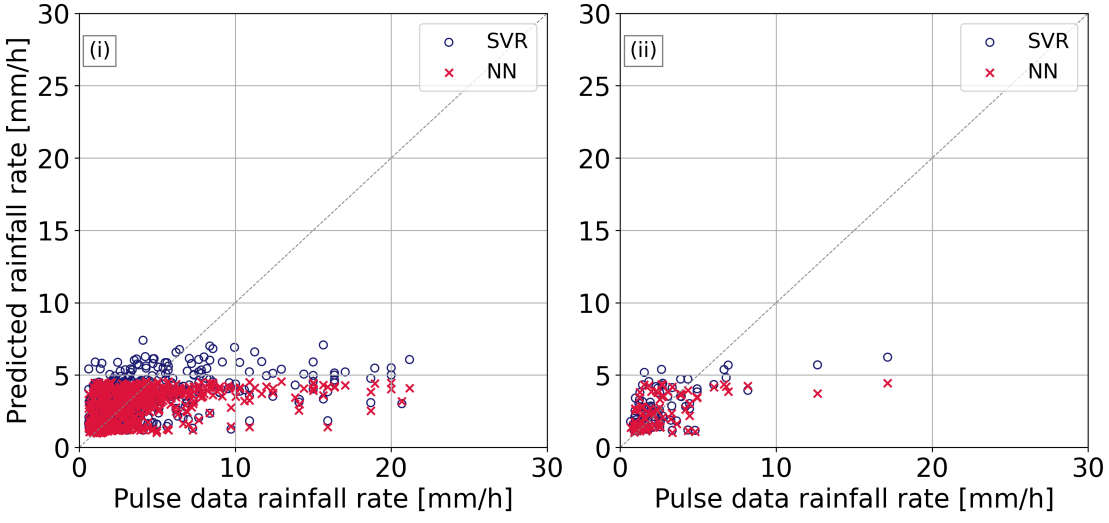

Figure A1. Scatter plots comparing predicted precipitation rate [mm/h] from SVR and NN models against pulse data precipitation rate [mm/h] for LCA radar. (i) corresponds to the training dataset and (ii) corresponds to the test dataset. Both plots are shown over a restricted range of 0–30 mm/h.

https://doi.org/10.5194/egusphere-2026-445
Preprint. Discussion started: 26 March 2026

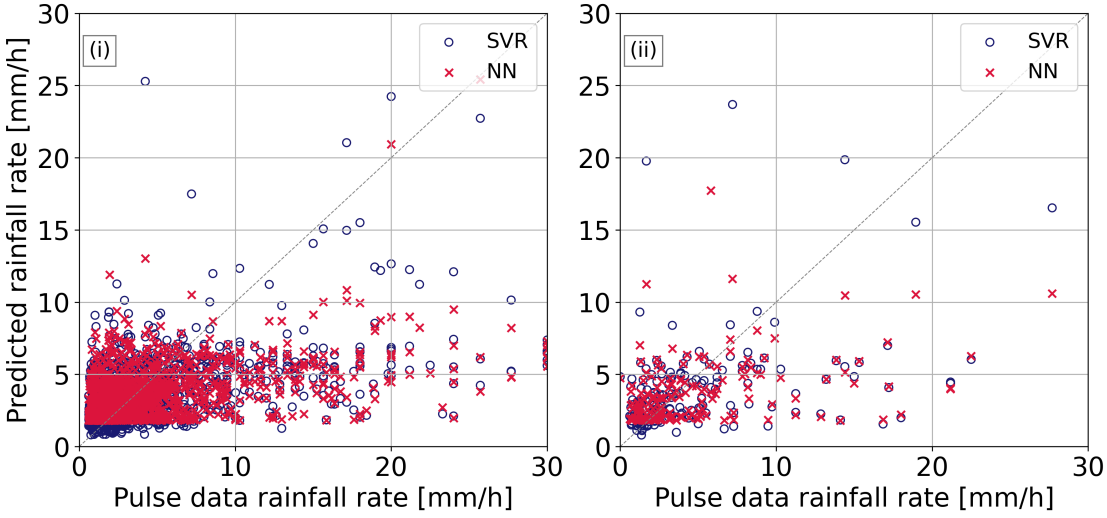

Figure A2. Scatter plots comparing predicted precipitation rate [mm/h] from SVR and NN models against pulse data precipitation rate [mm/h] for PFO radar. (i) corresponds to the training dataset and (ii) corresponds to the test dataset. Both plots are shown over a restricted range of 0–30 mm/h.

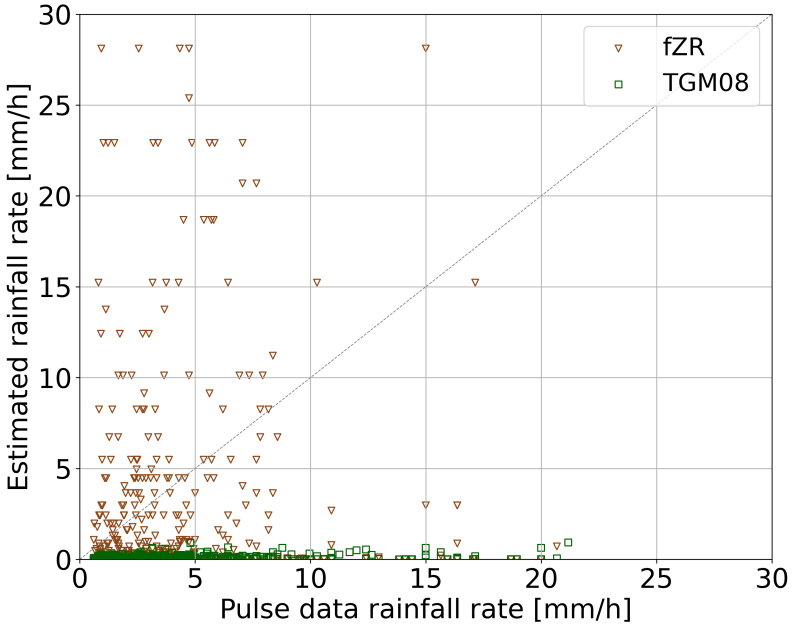

Figure A3. Scatter plot comparing pulse data rainfall rate [mm/h] with estimated rainfall rates from two methods: a fZR relationship (in brown) and the TGM08 relationship (in green) for LCA radar over a restricted range of 0–30 mm/h.

https://doi.org/10.5194/egusphere-2026-445
Preprint. Discussion started: 26 March 2026

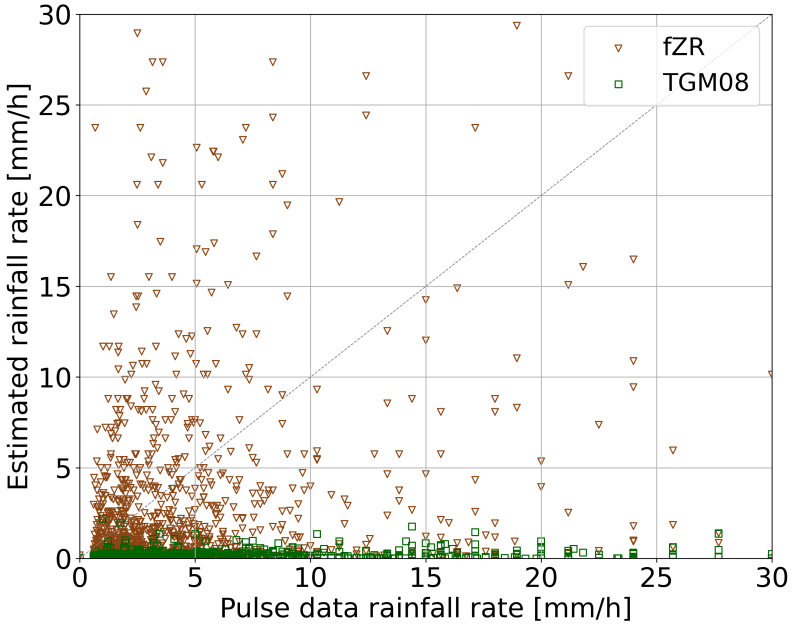

Figure A4. Scatter plot comparing pulse data rainfall rate [mm/h] with estimated rainfall rates from two methods: a fZR relationship (in brown) and the TGM08 relationship (in green) for PFO radar over a restricted range of 0–30 mm/h.

Author contributions. Conceptualization, E.L. and S.M.; methodology, E.L. and S.M.; software, E.L.; validation, S.M.; formal analysis, E.L.; investigation, E.L.; data curation, E.L.; writing—original draft preparation, E.L.; writing—review and editing, S.M. and D.H.; visualization, E.L.; supervision, D.H.; project administration, D.H.; funding acquisition, D.H. All authors have read and agreed to the published version of the manuscript.

Competing interests. No competing interests are present.

Acknowledgements. The authors acknowledge the "EXCELSIOR": ERATOSTHENES: EXcellence Research Centre for Earth Surveillance and Space-Based Monitoring of the Environment H2020 Widespread Teaming project (http://www.excelsior2020.eu). The "EXCELSIOR" project has received funding from the European Union's Horizon 2020 research and innovation programme under Grant Agreement No 857510, from the Government of the Republic of Cyprus through the Directorate General for the European Programmes, Coordination and Development, and the Cyprus University of Technology. The authors also acknowledge the Department of Meteorology of the Republic of Cyprus for providing the X-band radar data, as well as the rain gauge data.

https://doi.org/10.5194/egusphere-2026-445
Preprint. Discussion started: 26 March 2026

References

Alqudah, A., Chandrasekar, V., and Le, M.: Investigating rainfall estimation from radar measurements using neural networks, Natural Hazards and Earth System Sciences, 13, 535–544, https://doi.org/10.5194/nhess-13-535-2013, 2013.

Atlas, D. and Ulbrich, C. W.: Path- and Area-Integrated Rainfall Measurement by Microwave Attenuation in the 1–3 cm Band, Journal of Applied Meteorology and Climatology, 16, 1322 – 1331, https://doi.org/10.1175/1520-0450(1977)016<1322:PAAIRM>2.0.CO;2, 1977.

Ayzel, G., Scheffer, T., and Heistermann, M.: RainNet v1.0: a convolutional neural network for radar-based precipitation nowcasting, Geoscientific Model Development, 13, 2631–2644, https://doi.org/10.5194/gmd-13-2631-2020, 2020.

Bellerby, T., Todd, M., Kniveton, D., and Kidd, C.: Rainfall Estimation from a Combination of TRMM Precipitation Radar and GOES Multispectral Satellite Imagery through the Use of an Artificial Neural Network, Journal of Applied Meteorology, 39, 2115 – 2128, https://doi.org/10.1175/1520-0450(2001)040<2115:REFACO>2.0.CO;2, 2000.

Bringi, V. N. and Chandrasekar, V.: Polarimetric Doppler Weather Radar: Principles and Applications, Cambridge University Press, 2001.

Caseri, A. N., Santos, L. B. L., and Stephany, S.: A convolutional recurrent neural network for strong convective rainfall nowcasting using weather radar data in Southeastern Brazil, Artificial Intelligence in Geosciences, 3, 8–13, https://doi.org/10.1016/j.aiig.2022.06.001, 2022.

Chen, H., Chandrasekar, V., Tan, H., and Cifelli, R.: Rainfall Estimation From Ground Radar and TRMM Precipitation Radar Using Hybrid Deep Neural Networks, Geophysical Research Letters, 46, 10 669–10 678, https://doi.org/10.1029/2019GL084771, 2019.

Cheng, Y.-Y., Chang, C.-T., Chen, B.-F., Kuo, H.-C., and Lee, C.-S.: Extracting 3D Radar Features to Improve Quantitative Precipitation Estimation in Complex Terrain Based on Deep Learning Neural Networks, Weather and Forecasting, 38, 273 – 289, https://doi.org/10.1175/WAF-D-22-0034.1, 2023.

Christodoulou, C., Michaelides, S., Gabella, M., and Pattichis, C.: Prediction of rainfall rate based on weather radar measurements, vol. 2, pp. 1393 – 1396 vol.2, ISBN 0-7803-8359-1, https://doi.org/10.1109/IJCNN.2004.1380153, 2004.

Huangfu, J., Hu, Z., Zheng, J., Wang, L., and Zhu, Y.: Study on Quantitative Precipitation Estimation by Polarimetric Radar Using Deep Learning, Advances in Atmospheric Sciences, 41, 1147–1160, https://doi.org/10.1007/s00376-023-3039-0, 2024.

Iguchi, T., Seto, S., Meneghini, R., Yoshida, N., Awaka, J., Le, M., Chandrasekar, V., Brodzik, S., Kubota, T., and Takahashi, N.: GPM/DPR Level-2 Algorithm Theoretical Basis Document, NASA Technical Report, https://gpm.nasa.gov/resources/documents/gpm-dpr-level-2-algorithm-theoretical-basis-document-atbd, 2021.

Ivanov, S., Michaelides, S., Ruban, I., Charalambous, D., and Tymvios, F.: Impact of radar data assimilation on simulations of precipitable water with the Harmonie model: A case study over Cyprus, Atmospheric Research, 253, 105 473, https://doi.org/10.1016/j.atmosres.2021.105473, 2021.

Li, W., Chandrasekar, V., and Xu, G.: Investigations in radar rainfall estimation using neural networks, in: IGARSS 2003. 2003 IEEE International Geoscience and Remote Sensing Symposium. Proceedings (IEEE Cat. No.03CH37477), vol. 4, pp. 2347–2349 vol.4, https://doi.org/10.1109/IGARSS.2003.1294437, 2003.

Liu, M., Zuo, J., Tan, J., and Liu, D.: Comparing and Optimizing Four Machine Learning Approaches to Radar-Based Quantitative Precipitation Estimation, Remote Sensing, 16, https://doi.org/10.3390/rs16244713, 2024.

Loulli, E., Michaelides, S., Bühl, J., Loukas, A., and Hadjimitsis, D.: Calibration of Two X-Band Ground Radars Against GPM DPR Ku-Band, Remote Sensing, 17, https://doi.org/10.3390/rs17101712, 2025a.

https://doi.org/10.5194/egusphere-2026-445
Preprint. Discussion started: 26 March 2026

Loulli, E., Michaelides, S., Bühl, J., Loukas, A., and Hadjimitsis, D. G.: Correction of path integrated attenuation using data from two X-band ground-based radars and GPM, Atmospheric Research, 321, 108 080, https://doi.org/https://doi.org/10.1016/j.atmosres.2025.108080, 2025b.

Marshall, J. S. and Palmer, W. M. K.: The distribution of raindrops with size, Journal of Atmospheric Sciences, 5, 165–166, 1948.

Meneghini, R., Kim, H., Liao, L., Jones, J. A., and Kwiatkowski, J. M.: An Initial Assessment of the Surface Reference Technique Applied to Data from the Dual-Frequency Precipitation Radar (DPR) on the GPM Satellite, Journal of Atmospheric and Oceanic Technology, 32, 2281–2296, https://doi.org/10.1175/JTECH-D-15-0044.1, 2015.

Meneghini, R., Kim, H., Liao, L., Kwiatkowski, J., and Iguchi, T.: Path attenuation estimates for the GPM dual-frequency precipitation radar (DPR), Journal of the Meteorological Society of Japan, 99, 181–200, https://doi.org/10.2151/jmsj.2021-010, 2021.

Orlandini, S. and Morlini, I.: Artificial neural network estimation of rainfall intensity from radar observations, Journal of Geophysical Research Atmospheres, 105, 24 849–24 861, https://doi.org/10.1029/2000JD900408, 2000.

Osman, N. S. and Tahir, W.: Machine Learning-based Model for Enhanced Quantitative Precipitation Estimates (QPE) From Radar Images Extracted Features, in: 2023 IEEE 8th International Conference on Recent Advances and Innovations in Engineering (ICRAIE), pp. 1–5, https://doi.org/10.1109/ICRAIE59459.2023.10468103, 2023.

Peng, X., Li, Q., and Jing, J.: CNGAT: A Graph Neural Network Model for Radar Quantitative Precipitation Estimation, IEEE Transactions on Geoscience and Remote Sensing, 60, 1–14, https://doi.org/10.1109/TGRS.2021.3120218, 2022.

Rosenhoover, M., Rushing, J., Beck, J., White, K., and Graves, S.: Improving Doppler Radar Precipitation Prediction with Citizen Science Rain Gauges and Deep Learning, Sensors, 25, https://doi.org/10.3390/s25123719, 2025.

Tartaglione, N., Gabella, M., and Michaelides, S. C.: Short range forecast verification of convective rain for a night-time event over the area of Cyprus, Atmospheric Research, 88, 13–24, https://doi.org/10.1016/j.atmosres.2007.09.003, 2008.

Teschl, R., Randeu, W. L., and Teschl, F.: Improving weather radar estimates of rainfall using feed-forward neural networks, Neural Networks, 20, 519–527, https://doi.org/10.1016/j.neunet.2007.04.005, 2007.

Tsintikidis, D., Haferman, J., Anagnostou, E., Krajewski, W., and Smith, T.: A neural network approach to estimating rainfall from spaceborne microwave data, IEEE Transactions on Geoscience and Remote Sensing, 35, 1079–1093, https://doi.org/10.1109/36.628775, 1997.

Xiao, R. and Chandrasekar, V.: Development of a Neural Network Based Algorithm for Rainfall Estimation from Radar Observations, IEEE TRANSACTIONS ON GEOSCIENCE AND REMOTE SENSING, 35, 1997.

Xu, G. and Chandrasekar, V.: Operational feasibility of neural-network-based radar rainfall estimation, IEEE Geoscience and Remote Sensing Letters, 2, 13–17, https://doi.org/10.1109/LGRS.2004.842338, 2005.

Yang, H., Wang, T., Zhou, X., Dong, J., Gao, X., and Niu, S.: Quantitative estimation of rainfall rate intensity based on deep convolutional neural network and radar reflectivity factor, pp. 244–247, Association for Computing Machinery, ISBN 9781450371926, https://doi.org/10.1145/3358528.3358582, 2019.

Zhang, Y., Chen, S., Tian, W., and Chen, S.: Radar Reflectivity and Meteorological Factors Merging-Based Precipitation Estimation Neural Network, Earth and Space Science, 8, https://doi.org/10.1029/2021EA001811, 2021.